Search for neutrino-induced cascades with five years of AMANDA data

R. Abbasi, Y. Abdou, T. Abu-Zayyad, O. Actis, J. Adams, J.A. Aguilar, M. Ahlers, K. Andeen, J. Auffenberg, X. Bai, et al.

Accepted Manuscript

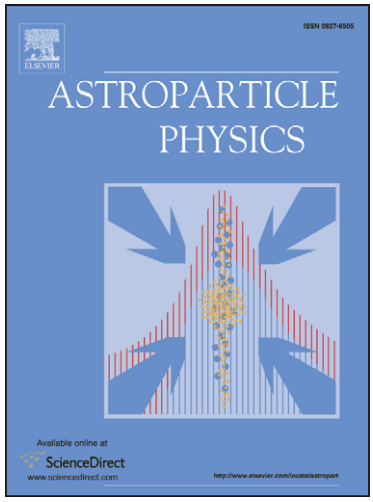

Search for neutrino-induced cascades with five years of AMANDA data

R. Abbasi, Y. Abdou, T. Abu-Zayyad, O. Actis, J. Adams, J.A. Aguilar, M. Ahlers, K. Andeen, J. Auffenberg, X. Bai, M. Baker, S.W. Barwick, R. Bay, J.L. Bazo Alba, K. Beattie, J.J. Beatty, S. Bechet, J.K. Becker, K.-H. Becker, M.L. Benabderrahmane, J. Berdermann, P. Berghaus, D. Berley, E. Bernardini, D. Bertrand, D.Z. Besson, M. Bissok, E. Blaufuss, D.J. Boersma, C. Bohm, S. Böser, O. Botner, L. Bradley, J. Braun, S. Buitink, M. Carson, D. Chirkin, B. Christy, J. Clem, F. Clevermann, S. Cohen, C. Colnard, D.F. Cowen, M.V. D'Agostino, M. Danninger, J.C. Davis, C. De Clercq, L. Demirörs, O. Depaepe, F. Descamps, P. Desiati, G. de Vries-Uiterweerd, T. DeYoung, J.C. Dı ´az-Vélez, J. Dreyer, J.P. Dumm, M.R. Duvoort, R. Ehrlich, J. Eisch, R.W. Ellsworth, O. Engdegård, S. Euler, P.A. Evenson, O. Fadiran, A.R. Fazely, T. Feusels, K. Filimonov, C. Finley, M.M. Foerster, B.D. Fox, A. Franckowiak, R. Franke, T.K. Gaisser, J. Gallagher, R. Ganugapati, M. Geisler, L. Gerhardt, L. Gladstone, T. Glüsenkamp, A. Goldschmidt, J.A. Goodman, D. Grant, T. Griesel, A. Groß, S. Grullon, R.M. Gunasingha, M. Gurtner, C. Ha, A. Hallgren, F. Halzen, K. Han, K. Hanson, K. Helbing, P. Herquet, S. Hickford, G.C. Hill, K.D. Hoffman, A. Homeier, K. Hoshina, D. Hubert, W. Huelsnitz, J.-P. Hülß, P.O. Hulth, K. Hultqvist, S. Hussain, R.L. Imlay, A. Ishihara, J. Jacobsen, G.S. Japaridze, H. Johansson, J.M. Joseph, K.-H. Kampert, A. Kappes, T. Karg, A. Karle, J.L. Kelley, N. Kemming, P. Kenny, J. Kiryluk, F. Kislat, S.R. Klein, S. Knops, J.-H. Köhne, G. Kohnen, H. Kolanoski, L. Köpke, D.J. Koskinen, M. Kowalski, T. Kowarik, M. Krasberg, T. Krings, G. Kroll, K. Kuehn, T. Kuwabara, M. Labare, S. Lafebre, K. Laihem, H. Landsman, R. Lauer, R. Lehmann, D. Lennarz, J. Lünemann, J. Madsen, P. Majumdar, R. Maruyama, K. Mase, H.S. Matis, M. Matusik, K. Meagher, M. Merck, P. Mészáros, T. Meures, E. Middell, N. Milke, J. Miller, T. Montaruli, R. Morse, S.M. Movit, R. Nahnhauer, J.W. Nam, U. Naumann, P. Nießen, D.R. Nygren, S. Odrowski, A. Olivas, M. Olivo, M. Ono, S. Panknin, L. Paul, C. Pérez de los Heros, J. Petrovic, A. Piegsa, D. Pieloth, R. Porrata, J. Posselt, P.B. Price, M. Prikockis, G.T. Przybylski, K. Rawlins, P. Redl, E. Resconi, W. Rhode, M. Ribordy, A. Rizzo, J.P. Rodrigues, P. Roth, F. Rothmaier, C. Rott, C. Roucelle, T. Ruhe, D. Rutledge, B. Ruzybayev, D. Ryckbosch, H.-G. Sander, S. Sarkar, K. Schatto, S. Schlenstedt, T. Schmidt, D. Schneider, A. Schukraft, A. Schultes, O. Schulz, M. Schunck, D. Seckel, B. Semburg, S.H. Seo, Y. Sestayo, S. Seunarine, A. Silvestri, A. Slipak, G.M. Spiczak, C. Spiering, M. Stamatikos, T. Stanev, G. Stephens, T. Stezelberger, R.G. Stokstad, S. Stoyanov, E.A. Strahler, T. Straszheim, G.W. Sullivan, Q. Swillens, I. Taboada, A. Tamburro, A. Tepe, S.

Ter-Antonyan, S. Tilav, P.A. Toale, D. Tosi, D. Turčan, N. van Eijndhoven, J. Vandenbroucke, A. Van Overloop, J. van Santen, B. Voigt, C. Walck, T. Waldenmaier, M. Wallraff, M. Walter, C. Wendt, S. Westerhoff, N. Whitehorn, K. Wiebe, C.H. Wiebusch, G. Wikström, D.R. Williams, R. Wischnewski, H. Wissing, K. Woschnagg, C. Xu, X.W. Xu, G. Yodh, S. Yoshida, P. Zarzhitsky

PII: S0927-6505(10)00204-5
DOI: 10.1016/j.astropartphys.2010.10.007
Reference: ASTPHY 1532

To appear in: *Astroparticle Physics*

Received Date: 9 June 2010
Revised Date: 10 September 2010
Accepted Date: 13 October 2010

Eijndhoven, J. Vandenbroucke, A. Van Overloop, J. van Santen, B. Voigt, C. Walck, T. Waldenmaier, M. Wallraff, M. Walter, C. Wendt, S. Westerhoff, N. Whitehorn, K. Wiebe, C.H. Wiebusch, G. Wikström, D.R. Williams, R. Wischnewski, H. Wissing, K. Woschnagg, C. Xu, X.W. Xu, G. Yodh, S. Yoshida, P. Zarzhitsky, Search for neutrino-induced cascades with five years of AMANDA data, *Astroparticle Physics* (2010), doi: 10.1016/j.astropartphys.2010.10.007

Search for neutrino-induced cascades with five years of AMANDA data

R. Abbasi[ab], Y. Abdou[v], T. Abu-Zayyad[ag], O. Actis[an], J. Adams[p], J. A. Aguilar[ab], M. Ahlers[af], K. Andeen[ab], J. Auffenberg[am], X. Bai[ae], M. Baker[ab], S. W. Barwick[x], R. Bay[g], J. L. Bazo Alba[an], K. Beattie[h], J. J. Beatty[r,s], S. Bechet[m], J. K. Becker[j], K.-H. Becker[am], M. L. Benabderrahmane[an], J. Berdermann[an], P. Berghaus[ab], D. Berley[q], E. Bernardini[an], D. Bertrand[m], D. Z. Besson[z], M. Bissok[a], E. Blaufuss[q], D. J. Boersma[a], C. Bohm[ah], S. Böser[k], O. Botner[ak], L. Bradley[aj], J. Braun[ab], S. Buitink[h], M. Carson[v], D. Chirkin[ab], B. Christy[q], J. Clem[ae], F. Clevermann[t], S. Cohen[y], C. Colnard[w], D. F. Cowen[aj,ai], M. V. D'Agostino[g], M. Danninger[ah], J. C. Davis[r], C. De Clercq[n], L. Demirörs[y], O. Depaepe[n], F. Descamps[v], P. Desiati[ab], G. de Vries-Uiterweerd[v], T. DeYoung[aj], J. C. Díaz-Vélez[ab], J. Dreyer[j], J. P. Dumm[ab], M. R. Duvoort[al], R. Ehrlich[q], J. Eisch[ab], R. W. Ellsworth[q], O. Engdegård[ak], S. Euler[a], P. A. Evenson[ae], O. Fadiran[d], A. R. Fazely[f], T. Feusels[v], K. Filimonov[g], C. Finley[ah], M. M. Foerster[aj], B. D. Fox[aj], A. Franckowiak[i], R. Franke[an], T. K. Gaisser[ae], J. Gallagher[aa], R. Ganugapati[ab], M. Geisler[a], L. Gerhardt[h,g], L. Gladstone[ab], T. Glüsenkamp[a], A. Goldschmidt[h], J. A. Goodman[q], D. Grant[u], T. Griesel[ac], A. Groß[p,w], S. Grullon[ab], R. M. Gunasingha[f], M. Gurtner[am], C. Ha[aj], A. Hallgren[ak], F. Halzen[ab], K. Han[p], K. Hanson[ab], K. Helbing[am], P. Herquet[ad], S. Hickford[p], G. C. Hill[ab], K. D. Hoffman[q], A. Homeier[i], K. Hoshina[ab], D. Hubert[n], W. Huelsnitz[q], J.-P. Hülß[a], P. O. Hulth[ah], K. Hultqvist[ah], S. Hussain[ae], R. L. Imlay[f], A. Ishihara[o], J. Jacobsen[ab], G. S. Japaridze[d], H. Johansson[ah], J. M. Joseph[h], K.-H. Kampert[am], A. Kappes[ab,1], T. Karg[am], A. Karle[ab], J. L. Kelley[ab], N. Kemming[i], P. Kenny[z], J. Kiryluk[h,g], F. Kislat[an], S. R. Klein[h,g], S. Knops[a], J.-H. Köhne[t], G. Kohnen[ad], H. Kolanoski[i], L. Köpke[ac], D. J. Koskinen[aj], M. Kowalski[k], T. Kowarik[ac], M. Krasberg[ab], T. Krings[a], G. Kroll[ac],

[1]affiliated with Universität Erlangen-Nürnberg, Physikalisches Institut, D-91058, Erlangen, Germany

[2]on leave of absence from Università di Bari and Sezione INFN, Dipartimento di Fisica, I-70126, Bari, Italy

[3]NASA Goddard Space Flight Center, Greenbelt, MD 20771, USA

K. Kuehn[r], T. Kuwabara[ae], M. Labare[m], S. Lafebre[aj], K. Laihem[a], H. Landsman[ab], R. Lauer[an], R. Lehmann[i], D. Lennarz[a], J. Lünemann[ac], J. Madsen[ag], P. Majumdar[an], R. Maruyama[ab], K. Mase[o], H. S. Matis[h], M. Matusik[am], K. Meagher[q], M. Merck[ab], P. Mészáros[ai,aj], T. Meures[a], E. Middell[an], N. Milke[t], J. Miller[ak], T. Montaruli[ab,2], R. Morse[ab], S. M. Movit[ai], R. Nahnhauer[an], J. W. Nam[x], U. Naumann[am], P. Nießen[ae], D. R. Nygren[h], S. Odrowski[w], A. Olivas[q], M. Olivo[ak,j], M. Ono[o], S. Panknin[i], L. Paul[a], C. Pérez de los Heros[ak], J. Petrovic[m], A. Piegsa[ac], D. Pieloth[t], R. Porrata[g], J. Posselt[am], P. B. Price[g], M. Prikockis[aj], G. T. Przybylski[h], K. Rawlins[c], P. Redl[q], E. Resconi[w], W. Rhode[t], M. Ribordy[y], A. Rizzo[n], J. P. Rodrigues[ab], P. Roth[q], F. Rothmaier[ac], C. Rott[r], C. Roucelle[w], T. Ruhe[t], D. Rutledge[aj], B. Ruzybayev[ae], D. Ryckbosch[v], H.-G. Sander[ac], S. Sarkar[af], K. Schatto[ac], S. Schlenstedt[an], T. Schmidt[q], D. Schneider[ab], A. Schukraft[a], A. Schultes[am], O. Schulz[w], M. Schunck[a], D. Seckel[ae], B. Semburg[am], S. H. Seo[ah], Y. Sestayo[w], S. Seunarine[l], A. Silvestri[x], A. Slipak[aj], G. M. Spiczak[ag], C. Spiering[an], M. Stamatikos[r,3], T. Stanev[ae], G. Stephens[aj], T. Stezelberger[h], R. G. Stokstad[h], S. Stoyanov[ae], E. A. Strahler[n], T. Straszheim[q], G. W. Sullivan[q], Q. Swillens[m], I. Taboada[e], A. Tamburro[ag], A. Tepe[e], S. Ter-Antonyan[f], S. Tilav[ae], P. A. Toale[aj], D. Tosi[an], D. Turčan[q], N. van Eijndhoven[n], J. Vandenbroucke[g], A. Van Overloop[v], J. van Santen[i], B. Voigt[an], C. Walck[ah], T. Waldenmaier[i], M. Wallraff[a], M. Walter[an], C. Wendt[ab], S. Westerhoff[ab], N. Whitehorn[ab], K. Wiebe[ac], C. H. Wiebusch[a], G. Wikström[ah], D. R. Williams[b], R. Wischnewski[an], H. Wissing[q], K. Woschnagg[g], C. Xu[ae], X. W. Xu[f], G. Yodh[x], S. Yoshida[o], P. Zarzhitsky[b]

[a] *III. Physikalisches Institut, RWTH Aachen University, D-52056 Aachen, Germany*
[b] *Dept. of Physics and Astronomy, University of Alabama, Tuscaloosa, AL 35487, USA*
[c] *Dept. of Physics and Astronomy, University of Alaska Anchorage, 3211 Providence Dr., Anchorage, AK 99508, USA*
[d] *CTSPS, Clark-Atlanta University, Atlanta, GA 30314, USA*
[e] *School of Physics and Center for Relativistic Astrophysics, Georgia Institute of Technology, Atlanta, GA 30332, USA*
[f] *Dept. of Physics, Southern University, Baton Rouge, LA 70813, USA*
[g] *Dept. of Physics, University of California, Berkeley, CA 94720, USA*
[h] *Lawrence Berkeley National Laboratory, Berkeley, CA 94720, USA*
[i] *Institut für Physik, Humboldt-Universität zu Berlin, D-12489 Berlin, Germany*
[j] *Fakultät für Physik & Astronomie, Ruhr-Universität Bochum, D-44780 Bochum, Germany*
[k] *Physikalisches Institut, Universität Bonn, Nussallee 12, D-53115 Bonn, Germany*

[l] Dept. of Physics, University of the West Indies, Cave Hill Campus, Bridgetown BB11000, Barbados
[m] Université Libre de Bruxelles, Science Faculty CP230, B-1050 Brussels, Belgium
[n] Vrije Universiteit Brussel, Dienst ELEM, B-1050 Brussels, Belgium
[o] Dept. of Physics, Chiba University, Chiba 263-8522, Japan
[p] Dept. of Physics and Astronomy, University of Canterbury, Private Bag 4800, Christchurch, New Zealand
[q] Dept. of Physics, University of Maryland, College Park, MD 20742, USA
[r] Dept. of Physics and Center for Cosmology and Astro-Particle Physics, Ohio State University, Columbus, OH 43210, USA
[s] Dept. of Astronomy, Ohio State University, Columbus, OH 43210, USA
[t] Dept. of Physics, TU Dortmund University, D-44221 Dortmund, Germany
[u] Dept. of Physics, University of Alberta, Edmonton, Alberta, Canada T6G 2G7
[v] Dept. of Subatomic and Radiation Physics, University of Gent, B-9000 Gent, Belgium
[w] Max-Planck-Institut für Kernphysik, D-69177 Heidelberg, Germany
[x] Dept. of Physics and Astronomy, University of California, Irvine, CA 92697, USA
[y] Laboratory for High Energy Physics, École Polytechnique Fédérale, CH-1015 Lausanne, Switzerland
[z] Dept. of Physics and Astronomy, University of Kansas, Lawrence, KS 66045, USA
[aa] Dept. of Astronomy, University of Wisconsin, Madison, WI 53706, USA
[ab] Dept. of Physics, University of Wisconsin, Madison, WI 53706, USA
[ac] Institute of Physics, University of Mainz, Staudinger Weg 7, D-55099 Mainz, Germany
[ad] Université de Mons, 7000 Mons, Belgium
[ae] Bartol Research Institute and Department of Physics and Astronomy, University of Delaware, Newark, DE 19716, USA
[af] Dept. of Physics, University of Oxford, 1 Keble Road, Oxford OX1 3NP, UK
[ag] Dept. of Physics, University of Wisconsin, River Falls, WI 54022, USA
[ah] Oskar Klein Centre and Dept. of Physics, Stockholm University, SE-10691 Stockholm, Sweden
[ai] Dept. of Astronomy and Astrophysics, Pennsylvania State University, University Park, PA 16802, USA
[aj] Dept. of Physics, Pennsylvania State University, University Park, PA 16802, USA
[ak] Dept. of Physics and Astronomy, Uppsala University, Box 516, S-75120 Uppsala, Sweden
[al] Dept. of Physics and Astronomy, Utrecht University/SRON, NL-3584 CC Utrecht, The Netherlands
[am] Dept. of Physics, University of Wuppertal, D-42119 Wuppertal, Germany
[an] DESY, D-15735 Zeuthen, Germany

Abstract

We report on the search for electromagnetic and hadronic showers ("cascades") produced by a diffuse flux of extraterrestrial neutrinos in the AMANDA

neutrino telescope. Data for this analysis were recorded during 1001 days of detector livetime in the years 2000 to 2004. The observed event rates are consistent with the background expectation from atmospheric neutrinos and muons. An upper limit is derived for the diffuse flux of neutrinos of all flavors assuming a flavor ratio of $\nu_e : \nu_\mu : \nu_\tau = 1 : 1 : 1$ at the detection site. The all-flavor flux of neutrinos with an energy spectrum $\Phi \propto E^{-2}$ is less than $5.0 \cdot 10^{-7}$GeV s^{-1} sr^{-1} cm^{-2} at a 90% C.L.. Here, 90% of the simulated signal would fall within the energy range 40 TeV to 9 PeV. We discuss flux limits in the context of several specific models of extraterrestrial and prompt atmospheric neutrino production.

Keywords: neutrinos, cascades

1. Introduction

The production of high-energy cosmic rays is most likely accompanied by astrophysical neutrinos [1]. High-energy neutrinos may be produced in astrophysical sources that accelerate protons and light nuclei and provide a dense environment of matter and radiation for interactions within or near the source. Source candidates include supernova remnants and micro-quasars in our Galaxy, as well as extragalactic sources such as Active Galactic Nuclei and Gamma-Ray Bursts (for a review, see [2, 3, 4]). For a generic astrophysical neutrino source, the neutrino flux is expected to be produced with a flavor ratio $\nu_e : \nu_\mu : \nu_\tau \sim 1 : 2 : 0$. After propagation to Earth, neutrino flavor mixing generally causes the ratio to be $1 : 1 : 1$ at the detection site [5]. Deviations to this equal partition are expected only for neutrino production in dense astrophysical environments or strong magnetic fields [6]. Because of the presence of all neutrino flavors in a cosmic neutrino beam, an ideal neutrino detector has sensitivity to all neutrino flavors.

The primary goal of the AMANDA detector was the search for extraterrestrial high-energy neutrinos. AMANDA was installed in the Antarctic ice cap at the geographical South Pole. The detector consisted of 677 optical modules (OMs) which were arranged in 19 vertical strings. The OMs were frozen into the ice at depths from 1500 m to 2000 m with a vertical separation of 20 m for strings 1 to 4 and 10-12 m for the other strings. The resulting instrumented volume formed a cylindrical geometry of about 200 m diameter and 500 m height. Each OM contained a photomultiplier tube (PMT) which recorded the Cherenkov light emitted by relativistic charged particles.

These particles were mainly high-energy muons produced in cosmic air showers as well as muons and other charged particles produced by neutrino-ice interactions in or near the detector volume. Analog signals from the OMs were transmitted to a surface data acquisition system (DAQ) where leading-edge times and amplitudes of the PMT pulses were digitized. The main AMANDA trigger, used here, retained only events with pulses from at least 24 OMs recorded within 2.5 μs.

In this paper, we present a search for a diffuse neutrino flux from unresolved astrophysical sources. Charged-current ν_e and ν_τ interactions, and neutral-current interactions of all three neutrino flavors, will produce electromagnetic and/or hadronic showers (so-called "cascades") in the ice. In contrast, charged-current ν_μ interactions produce a muon track. In AMANDA, electromagnetic and hadronic cascades are indistinguishable, although the average light level produced for a given shower energy is slightly different for each [7]. For cascades, the direction of the incoming neutrino is difficult to reconstruct to better than a few tens of degrees, but the calorimetric properties of the detector allow the energy of these events to be measured to better than 0.2 in the $\log_{10} E$ [8]. In the search for a diffuse high-energy neutrino flux, exclusion of track-like events eliminates most cosmic ray induced muon events, leaving mostly cascade-like events. An additional advantage in searching for cosmic ν_e and ν_τ compared to ν_μ is the fact that the flux of background atmospheric electron-neutrinos is more than an order of magnitude lower than the corresponding ν_μ flux and that the fluxes have different energy dependencies. The astrophysical high-energy neutrino sources are expected to have a spectrum of $\sim E^{-2}$ while the atmospheric flux decreases with $\sim E^{-3.7}$.

Previous efforts to search for neutrino-induced cascades [9] used data collected in 1997 with the 10-string AMANDA-B10 detector. A further search [8] used data taken in 2000 with the completed 19-string AMANDA detector. Other limits on the diffuse flux of astrophysical muon-neutrinos were derived by searching for track-like events [10] or by searching for events depositing a very large amount of energy [11]. These analyses used data from 2000-2003 and 2000-2002, respectively and are briefly discussed in section 4.5 below. With five years of data, this paper presents the final AMANDA results on the search for cascades from interactions of astrophysical neutrinos. In 2006, AMANDA was integrated into the IceCube neutrino telescope [12]. Data was taken by the combined detector for three years, until AMANDA was decommissioned in 2009.

Year	livetime (days)	Triggered Events	Trigger Rate (Hz)
2000	197	1.37×10^9	80.5
2001	193	2.00×10^9	120.0
2002	204	1.91×10^9	108.4
2003	213	1.86×10^9	101.1
2004	194	1.72×10^9	102.6
Total	1001	8.86×10^9	

Table 1: Effective detector livetime, number of triggered events and trigger rate for the 5 years of data used in the analysis. The year to year trigger rate variations are caused by changed settings of the photomultiplier voltages and discriminator thresholds as well as by modifications of other triggers than the high multiplicity trigger used for the cascade analysis.

2. Experimental Data and MC Simulation

The experimental data used here were recorded during the austral winters (February through November) in the years 2000 through 2004, i.e. they include the previously published year 2000 data of the cascade analysis [8]. Only data from periods with a stable operating detector were used for this analysis. This was a total livetime of 1001 days, after correction for DAQ deadtime between events. A total of $8.9 \cdot 10^9$ events were recorded at an average trigger rate of 103 Hz (Table 1). Although the yearly trigger rates in Table 1 differ by up to 20 %, the characteristics of the data, taken with the high multiplicity trigger, do not change appreciably. The different reconstruction steps will be described in the following section, but one of the essential cascade parameters is used here to illustrate the consistency between the annual data samples. Figure 1 shows the reconstructed energy of cascade candidates for the different years. There are only $\sim$5 % differences, which confirms that the data can be used for a combined 5-year analysis.

The data are dominated by the background of high-energy muons produced by cosmic ray interactions in the atmosphere. By removing track-like events, most of this atmospheric muon background can be eliminated. Muons may also lose energy by bremsstrahlung, direct pair production and photonuclear interactions. Therefore, a fraction of high-energy muons remain, mainly those that radiate energetic bremsstrahlung photons resembling cascade events. Since the atmospheric muon background simulation with the air shower simulation package CORSIKA [13] produces many lower-energy

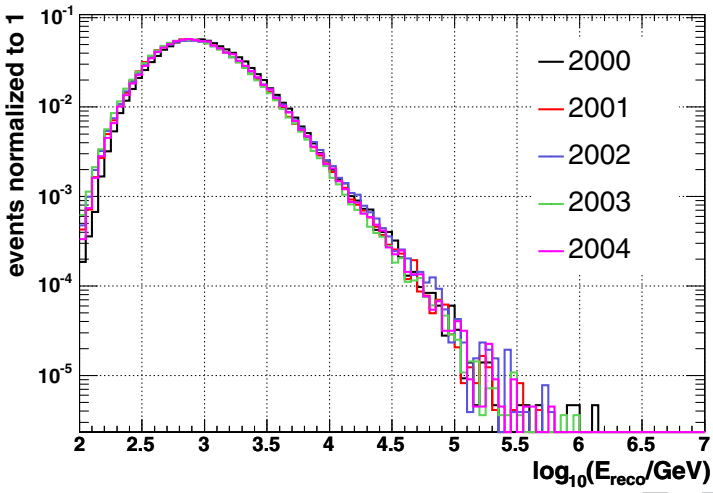

Figure 1: Reconstructed cascade energy for data of different years. For comparison, the curves are normalized to 1.

muons that do not radiate bremsstrahlung, computing time constraints made an optimization necessary to increase the statistics for high energy muons (see Table 2). The internal energy thresholds of CORSIKA were raised relative to those used in the standard AMANDA atmospheric muon simulation for the primary cosmic ray energy, the muon energy evaluated at the surface, and the energy released into a single secondary cascade near the AMANDA detector. For simulated events with more than one muon, these thresholds were applied to the highest energy muon and the secondary cascade which released the most energy. Two optimized samples were generated. The parameters of these simulations are summarized in Table 2, along with those of the standard simulation used in muon-focused AMANDA analyses. Figure 2 shows that the high-energy part of the spectrum is well represented by the optimized simulations. For the further analysis the second optimized sample with an equivalent livetime of 4670 days was used compared to 1001 days of real data.

Neutrino events of all flavors (ν_e, ν_μ, ν_τ) with energies between 100 GeV and 100 PeV were simulated with the neutrino generator code ANIS [14]. A general-purpose neutrino sample was produced with an E^{-1} spectrum with the neutrino interaction vertices uniformly distributed throughout the in-

BG sample	$E_{\rm cut}^{\rm primary}$	$E_{\rm cut}^{\mu}$	$E_{\rm cut}^{\rm secondary}$	Equivalent Livetime
standard	800 GeV	300 GeV	0.5 GeV	15 days
optimized sample 1	3 TeV	1.2 TeV	500 GeV	880 days
optimized sample 2	20 TeV	3.0 TeV	800 GeV	4670 days

Table 2: The atmospheric muon background samples used in this analysis. The equivalent livetime may be compared to the total detector livetime of 1001 days.

teraction volume. For this analysis the interaction volume was defined as a cylinder with a radius of 300 m and a height of ±300 m from the detector center. These events were then re-weighted to a hypothetical E^{-2} signal flux, as well as to several astrophysical neutrino model predictions with other energy spectra. For astrophysical neutrinos we assume equal flavor for neutrinos and antineutrinos. The steeper atmospheric neutrino spectrum was simulated by re-weighting the same events according to the atmospheric flux model [15], having a power law spectrum $\sim E^{-3.7}$.

In the next step of the simulation chain, for all events with final state muons (atmospheric background muons, signal and atmospheric background muon-neutrino events), the muons were propagated through the ice using the Muon Monte Carlo program MMC [16]. In this step the energy loss of muons due to ionization losses, bremsstrahlung, pair production, and photo-nuclear interactions is simulated.

3. Analysis

The goal of the analysis was to identify astrophysical neutrino-induced cascade events within the large background of atmospheric muon events. The analysis applied the same reconstruction algorithms to the experimental and simulated data sets. The algorithms were used already for the previous year 2000 cascade analysis [8]. To a good approximation, cascade events are point-like Cherenkov light emitters since the longitudinal cascade size of a few meters is short compared to the typical distance between OMs. Cherenkov light emission in ice peaks at an angle of 41° relative to the cascade longitudinal axis, but because of photon scattering in the ice, the directional information is mostly lost by the time of detection. Unlike cascades, muons typically

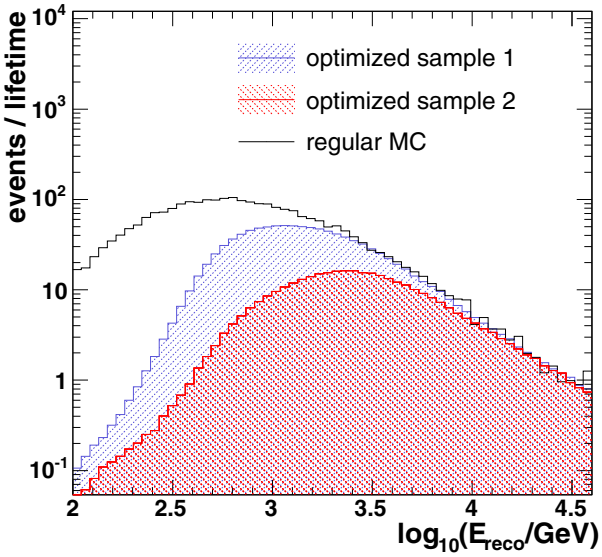

Figure 2: Reconstructed cascade energy for various background Monte Carlo samples. All events shown here have passed the vertex likelihood cut $L_{\text{vertex}} < 7.1$ (see the following section). At high energies, there is good agreement between the standard and the optimized samples.

leave long tracks of light along their path through the detector. Most of these muons can easily be rejected, but a fraction of muon tracks produce large bremsstrahlung cascades in the detector, leading to a cascade-like pattern of OM pulses ("hits"). In addition to hits from Cherenkov photons, uncorrelated random hits are caused by photomultiplier dark noise and electronics noise. Non-physics hits are also produced by cross-talk along the cables as well as in the surface electronics. A hit cleaning procedure removes most of the random and cross-talk hits prior to event reconstruction [17].

3.1. First Reconstruction Steps

Most of the nearly 9 billion triggered events are atmospheric muons which dominate clearly the background. A simple and fast reconstruction algorithm is needed to reduce the size of the data set. We used a fast 'first guess' event reconstruction with an analytic algorithm to estimate the cascade vertex position and time from the hit times and hit positions [8]. Two variables from this reconstruction were then used in the cascade event selection. The

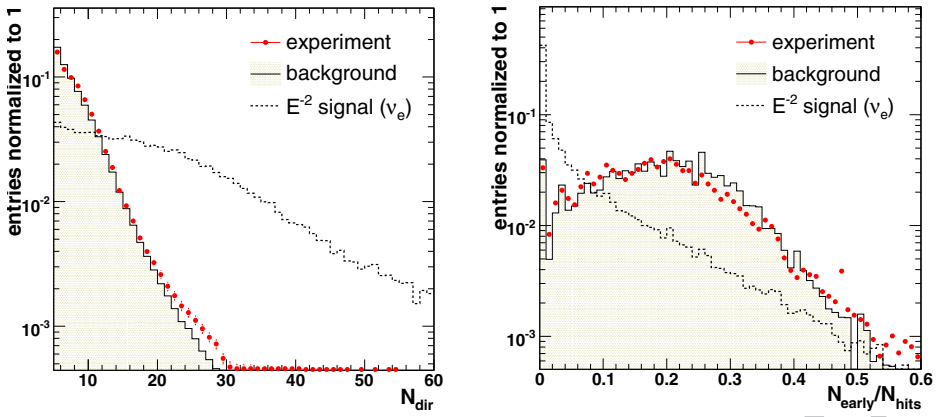

Figure 3: The two variables from a first-guess event reconstruction used in early data reduction for experimental data, signal and background Monte Carlo. Left: The number of direct hits N_{dir}, with time residuals $0 < t_{\mathrm{resid}} < 200\,ns$. Right: The ratio of early ($t_{\mathrm{resid}} < 0$) hits, N_{early}, to the total number of hits, N_{hits}.

first variable was the number N_{dir} of direct hits, defined as hits with times delayed relative to the arrival times expected for unscattered photons from the reconstructed interaction vertex by less than 200 ns. The second variable was N_{early}, the number of hits which occured earlier than the direct hits, that is hits with 'negative delay' times. The number of early hits should be small for real cascades, since such hits would violate causality for photons actually emitted at the cascade vertex position and time. Early hits in cascade events can only result from random dark noise, or from misreconstruction of the cascade vertex position. Relative to these incorrectly classified cascades, hits produced by light emitted farther back along the muon track will be classified as early hits. Figure 3 shows both variables for the data as well as for the simulated atmospheric muon background and signal. The cut values for the background reduction are presented in Table 3 together with the corresponding efficiencies. The large discrepancies between experimental data and simulated atmospheric muon background seen in table 3 are less visible in Fig. 3 due to the normalization. They are mainly caused by the simplified description of ice properties in the Monte Carlo simulation. The influence on the systematics error will be discussed in section 4.1.

3.2. Maximum Likelihood Methods

For events remaining after the cuts described above, the cascade vertex and the energy were reconstructed with more sophisticated maximum likelihood methods [9, 17, 18] which take into account the scattering and absorption of Cherenkov photons in ice.

3.2.1. Vertex Position Reconstruction

For the observation of the residual or delay time of photons ($t_{\rm res}$) as a function of the distance d between a hit OM and the reconstructed vertex position, a normalized probability density function (PDF) $\mathrm{p}(t_{\rm res}, d)$ was developed. This PDF allows to construct the likelihood function:

$$\mathcal{L} = \prod_{hit=1}^{all\ hits} p(t_{\rm res}, N, d), \quad L = \frac{-\log(\mathcal{L})}{N_{\rm hits} - N_{\rm free}}. \tag{1}$$

The vertex position and time are reconstructed by minimizing the likelihood function L in analogy to a reduced χ^2. $N_{\rm hits}$ is the total number of hits and $N_{\rm free} = 4$ is the number of free vertex parameters (3 space coordinates x, y, z and time t). The resulting vertex resolution is about 4 m in the transverse coordinates x, y and slightly better in the depth coordinate z.

3.2.2. Energy Reconstruction

A maximum likelihood method is also used for the energy reconstruction. Here, the likelihood is given by the probability to identify special hit patterns relevant for cascades. The hit-probability can be expressed by the number of expected photo-electrons η as a function of the distance d from an isotropically emitting point-like cascade:

$$\eta = I_0 \frac{E}{d} e^{-d/\lambda_{\rm att}}, \tag{2}$$

where $\lambda_{\rm att} = \sqrt{\lambda_{\rm scat}^{\rm eff} \lambda_{\rm abs}/3}$ is the attenuation length which is ~ 29 m for Cherenkov wave lengths. For distances larger than the photon scattering length, $d \gg \lambda_{scat}$, the information on the direction of the photon vanishes because of multiple scattering. The scattering of light is then described by the effective scattering length $\lambda_{\rm scat}^{\rm eff}$. The normalization constant I_0 depends on the OM orientation and the direction of the cascade.

With the expression for the expected number of photo-electrons one can calculate for each OM the probability to observe a hit:

$$P_{\rm hit}^{\rm casc} = 1 - P_{\rm nohit}^{casc} = 1 - e^{-\eta}, \tag{3}$$

For a realistic definition of the hit probability, one has to add the probability for the detection of noise hits:

$$P_{\rm hit} = 1 - P_{\rm nohit} = P_{\rm hit}^{\rm casc} + P_{\rm noise} - P_{\rm hit}^{\rm casc} P_{\rm noise}. \tag{4}$$

A likelihood function can be constructed as a product of the probability functions $P_{\rm hit}$ and $P_{\rm nohit}$:

$$\mathcal{L} = \prod_{i=1}^{\text{all hit OM}} P_{\rm hit}(E,d) \prod_{i=1}^{\text{all nohit OM}} P_{\rm nohit}(E,d), \tag{5}$$

$$L = -\frac{\mathcal{L}}{N_{\rm OM} - N_{\rm free}}. \tag{6}$$

$N_{\rm OM}$ is the total number of hit OMs and $N_{\rm free} = 1$ is the number of fit parameters. The resolution of the energy reconstruction is energy dependent. In $\log_{10} E$ units it is 0.13 at 100 GeV, rising to 0.22 at 1 PeV.

3.3. Selection Criteria for Likelihood Parameters and Vertex Position

The vertex and energy likelihood parameters were used for the further event selection. These variables contain the information about the quality of agreement between the best-fit hypothesis and the event. For the vertex position, the cut value is $L_{\rm vertex} < 7.1$. Since the cut variable $L_{\rm energy}$ is energy dependent, the cut criterion is:

$$L_{\rm energy} \leq \begin{cases} 1.1, & \log_{10}(\mathrm{E_{reco}}) \leq 3.9 \\ -0.625 \times \log_{10}(\mathrm{E_{reco}/GeV}) + 3.54, & \log_{10}(\mathrm{E_{reco}}) > 3.9 \end{cases}. \tag{7}$$

With the radial distance ρ_{xy} an additional cut variable was introduced which is defined as the distance of the cascade vertex from the central axis of the detector:

$$\rho_{xy} = \sqrt{x_{\rm reco}^2 + y_{\rm reco}^2} \tag{8}$$

The radial distance cut is softened in dependence on the cascade energy. For events inside the instrumented AMANDA detector volume of 100 meters radius, the energy cut is fixed to remove misreconstructed atmospheric muons.

For bright cascades (high energies), the background contamination is less severe and the cut is softened with increasing energy:

$$\rho_{\mathrm{xy}} \leq \begin{cases} 100 \text{ m}, & \log_{10}(\mathrm{E_{reco}}) \leq 3.1\mathrm{TeV} \\ 42.3 \times \log_{10}(\mathrm{E_{reco}}/\mathrm{GeV}) + 43.8 \text{ m}, & \log_{10}(\mathrm{E_{reco}}) > 3.1\mathrm{TeV} \end{cases} . \quad (9)$$

These three selection criteria are summarized in Table 3 with the corresponding cumulative cut efficiencies for data, background and signal events.

3.4. Final Selection Criteria

For the final event selection, three cut variables (see Fig. 4) were combined into a multivariate quality parameter. The first variable is the vertex likelihood parameter L_{vertex}, which possesses additional discriminative power after the cut shown in Table 3. The second variable ($\Delta\rho^{60}_{\mathrm{xy}}$) is the distance in the horizontal $x-y$ plane between vertex positions reconstructed with different hit selection criteria: $\Delta\rho^{60}_{\mathrm{xy}} = \sqrt{(x_{\mathrm{reco}} - x^{60}_{\mathrm{reco}})^2 + (y_{\mathrm{reco}} - y^{60}_{\mathrm{reco}})^2}$. In the first vertex reconstruction all hits were included; in the second, hits at a radius of more than 60 m from the first vertex were excluded. For a signal cascade event one expects only small differences in vertex position between the two reconstructions. Background muons that reach this stage of the analysis often have a bright bremstrahlung induced shower. For these events the difference $\Delta\rho^{60}_{\mathrm{xy}}$ is typically larger than for signal cascades. The third variable that enters the multivariate quality parameter is $\cos\theta_\mu$, where θ_μ is the zenith angle obtained by fitting the event to a muon track hypothesis. As can be seen in Fig. 4, the distribution peaks near $\cos\theta_\mu = 0$ for neutrino-induced cascades. When roughly spherical cascades are reconstructed as muon tracks in the tall cylindrical AMANDA detector, they appear mainly as horizontal tracks, whereas the atmospheric muon background is downward-going with $\cos\theta_\mu > 0$.

We combined the three variables shown in Fig. 4, into one quality variable, the likelihood ratio:

$$Q_{\mathrm{S}} = \frac{\prod_i p^s_i(x_i)}{\prod_i p^s_i(x_i) + \prod_i p^b_i(x_i)}, \quad (10)$$

where $0 < Q_{\mathrm{S}} < 1$ and i runs over the three variables $x_i = L_{\mathrm{vertex}}$, $\Delta\rho^{60}_{\mathrm{xy}}(E)$, $\cos\theta_\mu$. The functions p^s and p^b for signal and background, respectively, represent the probability density functions for the individual variables x_i for background due to atmospheric muons and signal consisting of a flux of ν_e

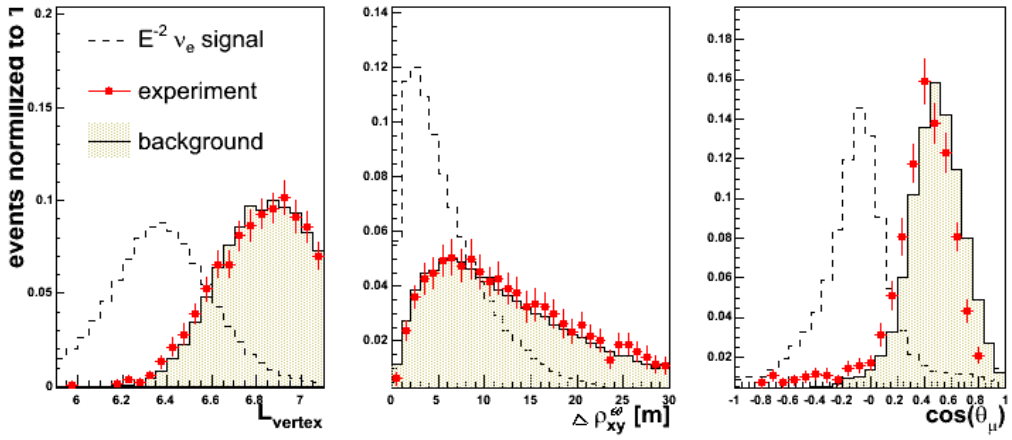

Figure 4: Distributions of three variables which are used to construct the discriminating likelihood parameter Q_{S} for the experimental data, the background and the signal MC. The left plot shows the vertex likelihood distribution. The plot in the middle shows the $\Delta\rho^{60}_{\mathrm{xy}}$ distributions. The plot on the right is the $\cos\theta_\mu$ distribution taken from the iterative muon likelihood reconstruction.

with a spectral slope $\Phi(E) \propto E^{-2}$. They are obtained from simulations and shown in Fig. 4.

The distribution of the variable Q_{S} (Fig. 5a) peaks close to one for the simulated cascade signal and close to zero for the simulated muon background (and experimental data). In addition to a cut on Q_{S}, which does not fully separate signal from background, the reconstructed cascade energy E_{reco} (Fig. 5b) was used to further reduce the background.

A discrete optimization procedure was used to find the cut values for Q_{S} and E_{reco} which maximized the separation of cascades from an E^{-2} neutrino spectrum from background muons. A two-dimensional grid was formed in the two variables, with bounds $0.90 < Q_{\mathrm{S}} < 0.99$ and $4.35 < \log_{10}(E_{\mathrm{reco}}\,/\mathrm{GeV}) < 6$ and step sizes of 0.01 and 0.05 respectively. At each grid point, the sensitivity, defined as the average upper limit for a ν_e flux in the absence of a signal [19], was calculated. The optimum sensitivity was found with the cuts $Q_{\mathrm{S}} > 0.92$ and $\log_{10}(E_{\mathrm{reco}}\,/\mathrm{GeV}) > 4.65$ yielding an average upper limit on the ν_e flux which will be given in section 4.4.

The efficiencies of all applied cuts are summarized in Table 3 for experimental data, the simulated background from atmospheric muons and at-

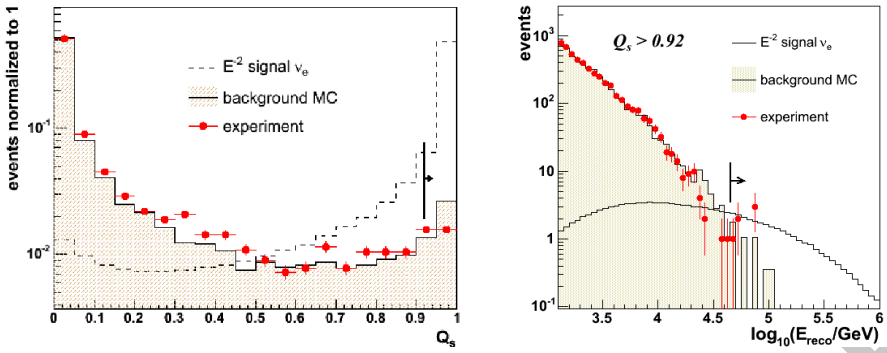

Figure 5: Distributions of the final cut variables Q_{S} and E_{reco} for the experimental data, for background and signal Monte Carlo. Left (a): The discriminating parameter Q_{S}. Right (b): The reconstructed cascade energy distribution E_{reco} after application of all quality cuts and a cut on the discriminating parameter $Q_{\mathrm{S}} > 0.92$. The signal Monte Carlo distribution is normalized to the lifetime of 1001 days and a flux $\Phi = 10^{-6}\, E^{-2}\mathrm{GeV\ s^{-1}\ sr^{-1}\ cm^{-2}}$.

mospheric neutrinos, and a hypothetical astrophysical electron-neutrino signal with a flux of $\Phi = 10^{-6}\, E^{-2}\mathrm{GeV\ s^{-1}\ sr^{-1}\ cm^{-2}}$ used as a benchmark for an extraterrestrial flux. All selection criteria were developed using only 20% of the experimental data, sampled evenly throughout the 5 years, and the remaining 80% were analyzed only after the cuts had been finalized in the manner described above. This blind analysis technique [20] was adopted to prevent possible biases in the selection procedure due to statistical fluctuations in the data. The results discussed in the following section were obtained with the full sample.

4. Results

4.1. Systematic Uncertainties

Several sources of systematic uncertainties must be evaluated and considered in calculating a limit on the astrophysical neutrino flux. Uncertainties in the detector parameter description and in the simulation and analysis chain were studied in detail in [17]. In the following we will discuss the major sources of systematic uncertainties in this analysis.

The detector configuration and trigger conditions changed slightly over the five year period, resulting in year-to-year variations in the event rate of

Cut Variable	Data	μ^{atm}	ν_e^{atm}	$E^{-2}\nu_e$ Signal
$N_{\rm early}/N_{\rm hits} < 0.05$	0.054	0.030	0.53	0.38
$N_{\rm dir} \geq 8$	0.032	0.015	0.49	0.33
$L_{\rm vertex} < 7.1$	6.5×10^{-4}	3.7×10^{-4}	0.32	0.24
$L_{\rm energy}(E)$	1.3×10^{-4}	1.0×10^{-4}	0.27	0.17
$\rho_{\rm xy}(E)$	8.7×10^{-5}	5.9×10^{-5}	0.12	0.10
$Q_{\rm S} > 0.92$	3.5×10^{-6}	2.1×10^{-6}	0.01	0.08
$\log_{10}(E_{\rm reco}\,/{\rm GeV}) > 4.65$	4.8×10^{-10}	5.2×10^{-10}	3.0×10^{-5}	0.02

Table 3: The cumulative cut efficiencies for experimental data, several types of background and an E^{-2} $(\nu_e + \bar{\nu}_e)$ signal. The cut variables $L_{\rm energy}$ and $\rho_{\rm xy}$ are energy dependent.

about 10 % after the different analysis steps. The variation of the optical module sensitivity as one possible source was investigated in detail for the years 2001 and 2003. For most of the strings the sensitivity was stable or the decrease was less than 10 %. The efficiency was about 20 % lower only for strings 1-4 in 2003. Since the strings operated with normal efficiency until the AMANDA shut-down in 2009, photocathode aging can be excluded. The reasons are changes of the high voltage and signal amplification settings. Averaging the variation in OM sensitivity over the full detector, the systematic uncertainty was estimated to be 13 %.

An essential component is the uncertainty in the modeling of photon propagation through the ice. A software package, PHOTONICS [21], was developed to simulate photon propagation through a turbid, translucent medium, taking into account the full wavelength and depth dependences of the scattering and absorption parameters. The required optical properties of deep ice at the South Pole have been measured by the AMANDA collaboration [22]. The inclusion of the full measured depth and wavelength dependencies in the photon propagation simulation results in very large lookup tables for use in the simulation of signal and background event topologies. Because of the computing time constraints to generate a large muon background sample, a much simplified simulation model PTD [23] was used in this analysis. In PTD the ice is divided into horizontal layers of homogeneous ice, such that each OM only sees a sheet of ice with depth-independent absorption and scattering properties typical of its own depth. In this approximation, the simulation propagates photons consequently through homogeneous ice only and are not subjected to the vertical variations in ice properties. An

additional simplification is that all photon scattering is modeled assuming an average wavelength of 420 nm. To investigate the uncertainty due to the simplified photon propagation in PTD, lower statistics Monte Carlo samples were generated using the more realistic PHOTONICS tables. A comparison of both photon propagation simulations yields uncertainties in event rate due to the photon propagation with PTD tables of 19 % for atmospheric muons, 23 % for atmospheric ν_μ and 28 % for atmospheric ν_e. For simulated E^{-2} signal events the uncertainty of 2 % is less crucial, since the higher energy of the signal events confers a certain amount of immunity to the specific optical properties of the ice. Meanwhile, PHOTONICS is the standard package for photon propagation in the ice of the AMANDA and IceCube detectors.

The reconstruction steps and selection criteria of the analysis (summarized in Table 3) yield different passing rates for data and simulated atmospheric muon background. Relaxing the Q_{S} cut for the background Monte Carlo sample to $Q_{\mathrm{S}} > 0.83$ results in the same efficiency as for the experimental data. The number of signal events increases by 12 %, which is taken as a measure of the uncertainty in the cut efficiency.

Finally, the theoretical uncertainties were considered. For the simulation of the atmospheric muon background there is uncertainty in the shape of the energy spectrum. Variations in the spectral energy slopes by $\Delta\gamma = 0.1$, a value somewhat larger than the current uncertainties [24], change the number of events passing the energy cut by 5 %, which is negligible relative to the other systematic and statistical uncertainties. Another theoretical uncertainty comes from the primary atmospheric neutrino flux prediction [25]. This uncertainty was estimated to be less than 20 % and does not contribute significantly to the total theoretical uncertainty, as the atmospheric neutrino event rate is a very small fraction of the total background rate. The 5 % uncertainty of the neutrino signal is caused by the uncertainty of the neutrino cross section at high energies [26]. In Table 4 the contributions to the systematic uncertainties are summarized and added in quadrature to get the total value.

4.2. Final Event Sample

After applying all cuts given in Table 3, six experimental events remain (see Fig. 5b). For these events the characteristic data and reconstructed variables are summarized in Table 6. The expected background at this final analysis level is 6.5 events, mostly from atmospheric muons (6.4 events) with

Systematic Uncertainty	$\Delta N_{\mu^{atm}}$	$\Delta N_{\nu_\mu^{atm}}$	$\Delta N_{\nu_e^{atm}}$	$\Delta N(E^{-2}\nu_e$ Signal)
Year-to-year variation	10 %	10 %	10 %	10 %
OM sensitivity	13 %	13 %	13 %	13 %
Cut efficiency	12 %	12 %	12 %	12 %
PTD ice model	19 %	23 %	28 %	2 %
Theoretical uncertainty	5 %	20 %	20 %	5 %
Total	28 %	37 %	40 %	21 %

Table 4: Different contributions to the systematic uncertainties of the number of events for the muon background, the atmospheric and signal neutrinos.

$N_{\rm Exp}$	$N_{\rm BG}^{\rm Total}$	$N_{\mu^{atm}}$	$N_{\nu_\mu^{atm}}$	$N_{\nu_e^{atm}}$	$N(E^{-2}\nu_e$ Signal)
6	$6.5^{+2.5}_{-2.4}$	$6.42^{+2.50}_{-2.40}$	0.065 ± 0.023	0.016 ± 0.006	20.9 ± 4.4

Table 5: The number of experimental events remaining after all cuts and the corresponding expected numbers of background and signal events from Monte Carlo simulations. The quoted errors include systematic uncertainties. For the ν_e signal a benchmark flux of $\Phi = 10^{-6}\, E^{-2}$GeV s^{-1} sr^{-1} cm^{-2} is assumed.

a small component from atmospheric muon neutrinos (0.065) and electron neutrinos (0.016).

Also shown in Fig. 5 is the expectation from the benchmark E^{-2} $(\nu_e + \bar{\nu}_e)$ signal Monte Carlo simulation. Normalized to the 1001 days of livetime, the final cut yields 20.9 signal ν_e events. Table 5 summarizes the final event numbers. The errors include the systematic uncertainties given in Table 4. Only the number of atmospheric muons has in addition a statistical error since the simulation was limited by statistics. This uncertainty was estimated with the upper and lower bounds for the 68.2 % C.L. using the method of Feldman and Cousins [19] to $N_{\mu^{atm}} = 6.4^{+1.8}_{-1.5}$ events.

Since no excess over the expected background was observed, an upper limit on the diffuse flux of astrophysical neutrinos was deduced. Following the method of Feldman and Cousins for constructing the confidence belt, the event upper limit before considering systematic uncertainties is $\mu = 4.99$ at 90% C.L. A Gaussian systematic error distribution was assumed for both signal and background. For the signal, the width is set to the estimated systematic uncertainty of $\pm 21\%$. Since the error distribution for the background is asymmetric, its peak position is chosen in the center of the uncertainty

Event #	1	2	3	4	5	6
Year	2002	2002	2002	2002	2003	2004
GPS day	179	181	273	285	129	56
V_x, m	14.62	19.08	84.92	1.19	26.59	51.9
V_y, m	111.64	103.72	7.89	125.36	-87.65	101.3
V_z, m	-95.64	-102.52	-48.12	-102.99	-126.70	-108.10
L_{vertex}	6.521	6.360	6.215	6.588	6.818	6.550
$\log_{10} E_{\mathrm{reco}}$, GeV	4.884	4.672	4.895	4.725	4.728	4.867
L_{energy}	0.663	0.591	0.586	0.772	1.089	0.596
$N_{\mathrm{early}}/N_{\mathrm{hits}}$	0.0231	0.0083	0.0001	0.0258	0.0070	0.0041
N_{direct}	23	16	29	30	16	62
N_{hits}	520	485	497	388	282	478
N_{ch}	227	208	267	188	175	208
Q_{s}	0.948	0.986	0.988	0.951	1.00	0.939

Table 6: The observables and reconstructed variables for the six events which passed all analysis cuts.

interval. The systematic uncertainties on the signal and background expectations were then included in the calculation of the event upper limit with the software package POLE++ [27]. This results in an event upper limit of 6.7 events at 90% confidence level.

4.3. AMANDA Effective Area

The sensitivity of the AMANDA detector to all three neutrino flavors can be expressed as an effective area. This measure incorporates the neutrino interaction probability, the detector sensitivity to events, the daughter lepton's range and the efficiency of the selection cuts. Neutrino event rates for any assumed neutrino flux can be computed from the effective area by integrating the flux times the effective area, with respect to energy.

Figure 6 shows the neutrino effective area of the AMANDA detector as a function of energy for $(\nu_e + \bar{\nu}_e)$, $(\nu_\mu + \bar{\nu}_\mu)$ and $(\nu_\tau + \bar{\nu}_\tau)$ for the present analysis averaged over $4\,\pi$ steradian. For $\overline{\nu}_e$, the peak around 6.3 PeV is the Glashow resonance, due to resonant production of W^- by neutrinos on atomic electrons. At 100 PeV the effective area reaches $0.3 - 0.8\,\mathrm{m}^2$, depending on the neutrino flavor.

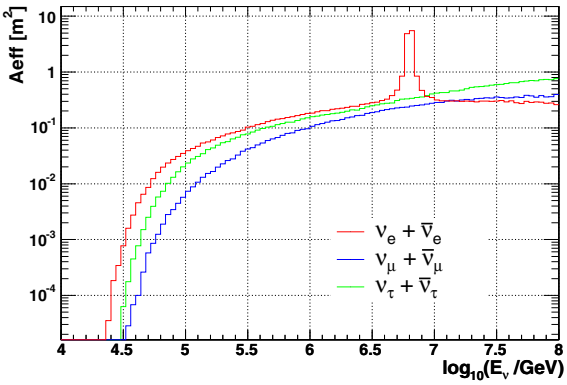

Figure 6: The neutrino effective areas for ν_e, ν_μ and ν_τ as a function of neutrino energy after all selection criteria have been applied.

Figure 7 shows the neutrino effective area for different zenith angle (θ) bands. Neutrino absorption in the Earth reduces the effective area for $\cos\theta < 0$ when $E_\nu \geq 100$ TeV. This also affects the Glashow resonance which is not visible for upward-going ($\nu_e + \bar{\nu}_e$). Tau neutrinos are not absorbed in the Earth but instead are regenerated, emerging with lower energies [28]. Because of this, the effective area for upward-going ν_τ does not decrease with higher energies.

4.4. Flux Upper Limit

The upper limit of 6.7 events deduced in Section 4.2 was combined with the effective area to constrain neutrino flux models. For a given model, we computed the ratio of the event upper limit to the expected neutrino event rate for that model. If this ratio, the Model Rejection Factor (MRF) [29], is less than one, the model is ruled out by the data at 90% CL. For example, an E^{-2} power law total flux of neutrinos of all flavors, $\Phi = 10^{-6} E^{-2} \mathrm{GeVs}^{-1}\mathrm{sr}^{-1}\mathrm{cm}^{-2}$, distributed equally over all neutrino flavors would produce 7.0 events due to electron-neutrinos i.e. 1/3 of the value from Table 5, 2.3 due to muon-neutrinos, and 4.0 due to tau-neutrinos for a total of 13.3 neutrino events. Comparing these 13.3 events to the experimental limit of 6.7 events, one obtains an MRF of 0.5. Rescaling the model flux by the MRF leads to the flux upper limit $E^2\Phi_{90\%\mathrm{CL}} \leq 5.0 \cdot 10^{-7} \mathrm{GeVs}^{-1}\mathrm{sr}^{-1}\mathrm{cm}^{-2}$. For this spectrum, the central 90% of the ν_e signal events would fall into the energy range 40 TeV

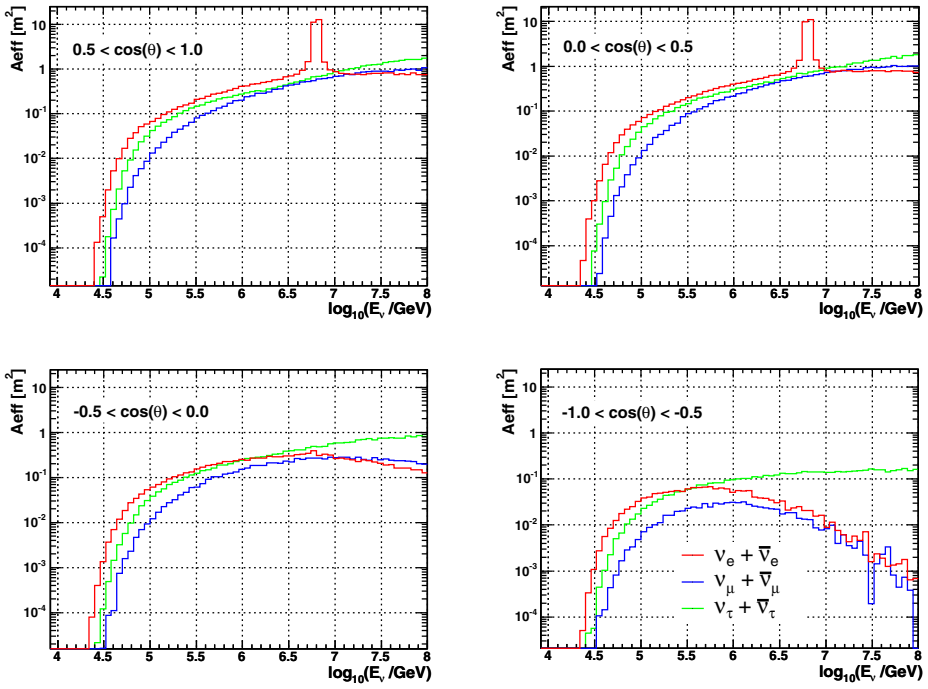

Figure 7: The neutrino effective area for AMANDA as a function of the neutrino energy for four different ranges of the zenith angle. Distributions for electron-, muon- and tau-neutrinos are shown separately. The tau regeneration effect is mainly visible in the two lower plots, which are for up-going neutrinos.

to 9 PeV. This upper limit on the total flux assumes a flavor ratio of $1:1:1$ and is equivalent to a limit of $E^2\Phi_{90\%\mathrm{CL}} \leq 1.7 \cdot 10^{-7}\mathrm{GeVs}^{-1}\mathrm{sr}^{-1}\mathrm{cm}^{-2}$ on each individual neutrino flavor. A more conservative upper limit on the flux of electron neutrinos that does not depend on the assumption of a $1:1:1$ flavor ratio is derived by assuming that the ν_μ and ν_τ fluxes are zero. An upper limit of $E^2\Phi_{\nu_e} \leq 3.3 \cdot 10^{-7}\,\mathrm{GeVs}^{-1}\mathrm{sr}^{-1}\mathrm{cm}^{-2}$ at 90% C.L was obtained.

Table 7 presents the expected number of events in 1001 days of livetime and the corresponding MRFs for several models of neutrino production in astrophysical sources and in the atmosphere. The spectra predicted by these models are shown in Fig. 8. With the exception of the Waxman-Bahcall model for neutrino production in GRBs [32], the astrophysical models con-

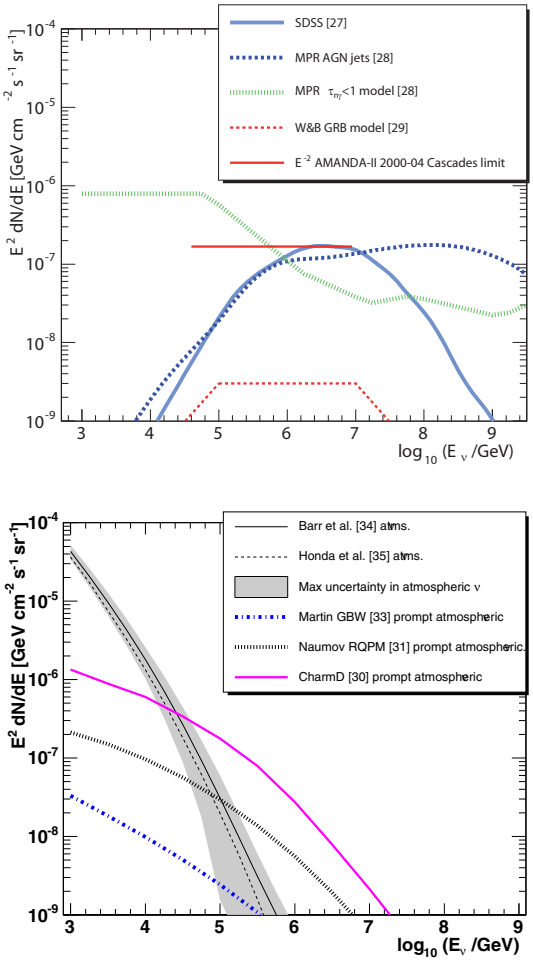

Figure 8: Flux prediction per neutrino flavor. a) For several models of astrophysical neutrino sources. b) For atmospheric neutrinos from pion and kaon decays and due to charm production. Table 7 gives the Model Rejection Factors for the individual models.

sider neutrino production in AGN. The model by Mannheim, Protheroe and Rachen [31] provides an upper bound for AGN sources optically thin to neutrons (optical depth $\tau < 1$). Since for this model the MRF is less than one, our experimental data can exclude this model, with most of the discrimination power derived from the region below 0.5 PeV. For the other astrophysical model predictions that were tested [30, 31, 32], the MRFs are greater than

Model	$\nu_e + \bar{\nu}_e$	$\nu_\mu + \bar{\nu}_\mu$	$\nu_\tau + \bar{\nu}_\tau$	all-flavors	MRF
$10^{-6}E^{-2}$	6.97	2.32	3.99	13.30	0.50
SDSS (2005) [30]	1.08	0.37	0.60	2.05	2.58
MPR (AGN jet) [31]	1.07	0.50	0.72	2.29	2.29
MPR ($\tau < 1$)[31]	8.52	7.56	2.77	18.85	0.28
WB GRB [32]	0.03	0.02	0.01	0.06	89.50
Charm D [33]	2.06	0.68	-	2.74	1.92
Naumov RQPM [34]	0.42	0.15	-	0.57	9.24
Martin GBW [36]	0.04	0.01	-	0.05	112.34

Table 7: Summary of the expected number of events in 1001 days of lifetime from various astrophysical and atmospheric prompt neutrino models. A flux ratio of $1 : 1 : 1$ is assumed. For the event upper limit the estimated value of $\mu_{90\%} = 6.7$ is used which includes all systematic uncertainties.

one, i.e. the AMANDA flux upper limits do not constrain these other models.

This analysis is also sensitive to atmospheric electron- and muon-neutrinos produced in decays of short lived charmed mesons, the so-called prompt neutrinos, which have a harder spectrum than the conventional flux of atmospheric neutrinos. The model with the highest flux prediction that is considered here is based on a non-perturbative calculation for the cross section [33], would result in 2.7 events and is therefore close to being constrained. This model was ruled out by the previous AMANDA diffuse ν_μ study [10]. Other models for prompt neutrino production [34, 36] predict significantly lower event rates and are hence not constrained by our data.

4.5. Comparison with other Results

This five years cascade analysis has an about 60 % higher sensitivity than the result published for the year 2000 [8]. The reconstruction algorithms and the selection criteria for cascade-like events were almost identical in both analyses. The five times larger number of triggered events and the considerably higher equivalent live time for the atmospheric muon background sample of about 4700 days allowed to improve the neutrino energy range. In Table 8, the essential parameters are summarized also for other diffuse analyses of the AMANDA and Baikal experiments. Fig. 9 shows the corresponding flux limits and the validity regions in neutrino energy.

The search for a diffuse flux of muon neutrinos [10] was performed for the

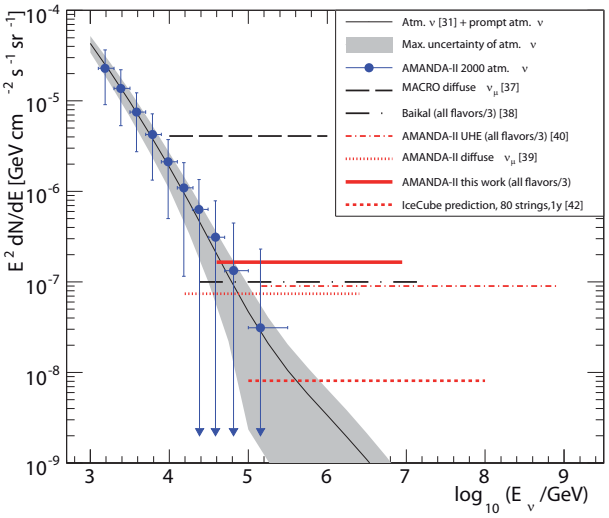

Figure 9: The upper limit on a diffuse neutrino flux from sources with an E^{-2} energy spectrum are shown for muon neutrinos and all-flavor analyses. All-flavor upper limits were divided by three, assuming the flavor ratio at the Earth to be $\nu_e + \bar{\nu}_e : \nu_\mu + \bar{\nu}_\mu : \nu_\tau + \bar{\nu}_\tau \approx 1 : 1 : 1$.

years 2000 to 2003. In contrast to the cascade analysis, one searches for upgoing muon tracks in the AMANDA detector resulting from neutrinos which interact with the rock or the ice below the detector. The essential final cut parameter is the number of hit optical modules ($N_{\rm ch} > 100$) which is equivalent to an energy cut. It allows to separate astrophysical high energy neutrinos from lower energetic atmospheric neutrinos or misreconstructed muons which are the main background contributions. Applying this cut, 6 events remain in the data sample in good agreement with the expected number of 7 atmospheric neutrino events.

The focus of the other AMANDA diffuse neutrino analysis was the ultra-high-energy (UHE) part of the spectrum [11]. For energies above $10^7\,GeV$, the Earth becomes opaque to neutrinos. Therefore, this analysis investigates neutrinos reaching the detector from directions near to the horizon. At these energies the background of atmospheric neutrinos can be neglected, but bundles of atmospheric muons can produce enough light in the detector similar to UHE neutrino events. Monte Carlo studies have shown that OMs

Analysis	ν Flavors	Livetime (days)	Energy Range (PeV)	Sensitivity Limit
Cascades (this analysis)	ν_e, ν_μ, ν_τ	1001	0.040 - 9	$\leq 5.0 \cdot 10^{-7}$
Cascades [8]	ν_e, ν_μ, ν_τ	197	0.050 - 5	$\leq 8.6 \cdot 10^{-7}$
Diffuse ν_μ [10]	ν_μ	807	0.016 - 2.5	$\leq 7.4 \cdot 10^{-8}$
UHE ν [11]	ν_e, ν_μ, ν_τ	457	0.200 - 1000	$\leq 2.7 \cdot 10^{-7}$
Cascades [41] (Baikal exp.)	ν_e, ν_μ, ν_τ	1038	0.020 - 20	$\leq 2.7 \cdot 10^{-7}$

Table 8: Comparison of this cascade analysis with published results from different diffuse analyses of the AMANDA experiment and of the Baikal experiment. The upper limit of the sensitivity is defined as $E^2\Phi \leq$ ..... GeVs^{-1} sr^{-1} cm^{-2} at 90% C.L..

have more single hits for background muon bundles, whereas UHE neutrinos produce more multiple hits. In this analysis all three neutrino flavors are considered, which leads to a separation of cascade-like and muon-like events at higher reconstruction levels. After all selection criteria remain 1 data and 1.3 background events yielding the excellent diffuse all-flavour neutrino flux limit.

The Baikal experiment has published a search for diffuse neutrinos [41] where data are analyzed taken between 1998 and beginning of 2003. Their cascade analysis has the advantage that the scattering of Cherenkov photons is rather small in the water of the Lake Baikal which allows the reconstruction of the shower direction. This results in an improved background suppression and in a total all-flavor flux limit which is slighly better than the limit of our analysis.

5. Conclusions

A search for neutrino-induced cascades in 1001 days of AMANDA data yielded a result consistent with cosmic ray induced atmospheric background. From this non-detection of an excess we derive an upper limit on the diffuse flux of astrophysical neutrinos with a spectrum $\Phi \propto E^{-2}$, as well as for other astrophysically motivated spectra. This analysis is sensitive to all three neutrino flavors. Since neutrino oscillations generally results in an equal flux of neutrinos of all three flavors at Earth [5], we constrain the total flux of

astrophysical neutrinos to $E^2\Phi \leq 5.0 \cdot 10^{-7}\,\mathrm{GeVs}^{-1}\,\mathrm{sr}^{-1}\,\mathrm{cm}^{-2}$ at 90% C.L. for a neutrino energy spanning 40 TeV to 9 PeV.

As shown in Fig. 9, the limit from this five year analysis, which is mainly sensitive to ν_e and ν_τ, provides competitive constraints on the flux of electron neutrinos and on the flux of all neutrino flavors. These new results for the limit and for the effective area are more stringent and supersede the older ones based on the data taken in the year 2000.

Since 2005 the IceCube neutrino telescope [12] is under construction, which once completed in 2011 will have an instrumented volume of one cubic kilometer. The search for a diffuse neutrino flux using the signature of isolated cascades is expected to significantly profit from the larger size and the improved readout technology of IceCube. First results, however not a limit, were presented for the 22 string IceCube data taken in 2007 [42]. For astrophysical neutrited when a 1-km^{3}yr exposure is reached [43].

Acknowledgements

We acknowledge the support from the following agencies: U.S. National Science Foundation-Office of Polar Program, U.S. National Science Foundation-Physics Division, University of Wisconsin Alumni Research Foundation, U.S. Department of Energy, and National Energy Research Scientific Computing Center, the Louisiana Optical Network Initiative (LONI) grid computing resources; Swedish Research Council, Swedish Polar Research Secretariat, and Knut and Alice Wallenberg Foundation, Sweden; German Ministry for Education and Research (BMBF), Deutsche Forschungsgemeinschaft (DFG), Research Department of Plasmas with Complex Interactions (Bochum), Germany; Fund for Scientific Research (FNRS-FWO), FWO Odysseus programme, Flanders Institute to encourage scientific and technological research in industry (IWT), Belgian Federal Science Policy Office (Belspo); Marsden Fund, New Zealand; M. Ribordy acknowledges the support of the SNF (Switzerland); A. Kappes and A. Groß acknowledge support by the EU Marie Curie OIF Program; J. P. Rodrigues acknowledge support by the Capes Foundation, Ministry of Education of Brazil.

References

References

[1] F.W. Stecker, C. Done, M.H. Salomon and P. Sommers, Phys. Rev. Lett. 66 (1991) 2697.

[2] F. Halzen and D. Hooper, Rept. Prog. Phys. 65 (2002) 1025 and astro-ph/0204527v2.

[3] J. Becker, Phys. Rept. 458 (2008) 173 and arXiv:0710.1557v2.

[4] L.A. Anchordoqui, D. Hooper, S. Sarkar and A.M. Taylor, Astropart. Phys. 29 (2008) 1 and astro-ph/0703001.

[5] J.G. Learned and S. Pakvasa, Astropart. Phys. 3 (1995) 267.

[6] T. Kashti and E. Waxman, Phys. Rev. Lett. 95 (2005) 181101 and astro-ph/0507599.

[7] M. Kowalski, Ph.D. thesis, Humboldt-Universität, Berlin (2003), http://edoc.hu-berlin.de/dissertationen/kowalski-marek-paul-2004-01-13/ PDF/Kowalski.pdf

[8] M. Ackermann et al., AMANDA Collaboration, Astropart. Phys. 22 (2004) 127.

[9] J. Ahrens et al., AMANDA Collaboration, Phys. Rev. D 67 (2003) 12003.

[10] A. Achterberg et al., AMANDA Collaboration, Phys. Rev. D 76 (2007) 42008.

[11] M. Ackermann et al., AMANDA Collaboration, Astrophysical Journal 675 (2008) 1014.

[12] A. Achterberg et al., IceCube Collaboration, Astropart. Phys. 26 (2006) 155.

[13] D. Heck, G. Schatz, T. Thouw, J. Knapp and J.N. Capdevielle, Technischer Report 6019, Forschungszentrum Karlsruhe, Germany (1998), http://www-ik.fzk.de/corsika.

[14] A. Gazizov and M. Kowalski, Comput. Phys. Commun. 172 (2005) 203.

[15] P. Lipari, Astropart. Phys. 1 (1993) 195.

[16] D. Chirkin and W. Rhode, arXiv:hep-ph/0407075v1 (2004).

[17] O. Actis, Ph.D. thesis, Humboldt-Universität, Berlin (2007), http://edoc.hu-berlin.de/docviews/abstract.php?lang=ger&id=29531.

[18] M. Kowalski and I. Taboada for the AMANDA Collaboration, 2nd Workshop Methodical Aspects of Underwater/Underice Telescopes, Hamburg, Germany (2001).

[19] G. Feldman and R. Cousins, Phys. Rev. D 57 (1998) 3873.

[20] J.R. Klein and A. Roodman, Ann. Rev. of Nucl. and Part. Science 55 (2005) 141.

[21] J. Lundberg et al., Nucl.Instrum.Meth. A 581 (2007) 619.

[22] M. Ackermann et al., AMANDA Collaboration, Journal of Geophysical Research 111 (2006) D13203.

[23] A. Karle for the AMANDA Collaboration, Proceedings of the International Workshop on Simulations and Analysis Methods for Large Neutrino Telescopes, DESY in Zeuthen, Germany (1998).

[24] J.R. Hörandel, Astropart. Phys. 19 (2003) 193.

[25] T.K. Gaisser and M.Honda, Ann. Rev. Nucl. Part. Sci. 52 (2002) 153.

[26] R. Gandhi, C. Quigg, M.H. Reno and I.Sarcevic, Astropart. Phys. 5 (1996) 81.

[27] J. Conrad, O. Botner, A. Hallgren and C. Perez de los Heros, Phys. Rev. D 67 (2003) 12002.

[28] O.B. Bigas, O. Deligny, K. Payet and V. Van Elewyck, Phys. Rev. D 78 (2008) 063002.

[29] G.C. Hill and K. Rawlins, Astropart. Phys. 19 (2003) 393.

[30] F.W. Stecker, Phys. Rev. D 72 (2005) 107301.

[31] K. Mannheim, R.J. Protheroe and J.P. Rachen, Phys. Rev. D 63 (2000) 23003.

[32] E. Waxman and J. Bahcall, Phys. Rev. Lett. 78 (1997) 2292.

[33] E. Zas, F. Halzen and R.A. Vazquez, Astropart. Phys. 1 (1993) 297.

[34] E. V. Bugaev, V. A. Naumov, S. I. Sinegovsky and E. S. Zaslavskaya, Nuovo Cim. 12 (1989) 41 and arXiv:hep-ph/0201310.

[35] G. Fiorentini et al., Macro Collaboration, Phys. Lett. B 510 (2001) 173.

[36] A.D. Martin et al., Acta Phys. Polon. B 34 (2003) 3273.

[37] G.D. Barr et al., Phys. Rev. D 70 (2004) 23006, and astro-ph/0611266 (2006).

[38] M. Honda et al., Phys. Rev. D 70 (2004) 43008 and astro-ph/0404457 (2004).

[39] K. Münich for the IceCube Collaboration, Proc. of the 29. ICRC, Pune, India (2005), astro-ph/0509330.

[40] M. Ambrosio et al., MACRO Collaboration, Astropart. Phys. 19 (2003) 1.

[41] A.V.Avrorin et al., Baikal Collaboration, Astronomy Letters 35, No. 10 (2009) 651.

[42] J. Kiryluk for the IceCube Collaboration, Proc. of the 31. ICRC, Lodz, Poland (2009), arXiv:astro-ph.HE/0909.0989v1 (2009), to be published.

[43] M. Kowalski, JCAP 05 (2005) 10.